

Investigation into Linear Micropattern Generation using Electrochemical Micromachining

S. Kunar^{1,2,*}, P. P. Das³, A. P. Tiwary³, Veeranjanyulu Itha^{1,2}, Norfazillah Talib⁴, S. Rama Sree^{2,5} and M. S. Reddy^{1,2}

¹Department of Mechanical Engineering, Aditya Engineering College, Surampalem, India

²Jawaharlal Nehru Technological University Kakinada, Kakinada, East Godavari, India

³Department of Mechanical Engineering, Sikkim Manipal Institute of Technology, Sikkim Manipal University, Sikkim, India

⁴Department of Manufacturing Engineering, Faculty of Mechanical and Manufacturing Engineering, Universiti Tun Hussein Onn Malaysia, 86400 Batu Pahat, Johor, Malaysia

⁵Department of Computer Science & Engineering, Aditya Engineering College, Surampalem, India

Received 5 June 2021; Accepted 22 August 2022

Abstract

Micropatterned surfaces perform a significant role in the performance of microfabricated devices. Maskless electrochemical micromachining (EMM) is a unique prevalent technique for creating linear micropatterns with precise geometric dimensions and surface quality. However, this method is an advanced micromachining method for fabricating linear micropatterns in comparison to traditional EMM and photolithography, both being costly during mass production. This advanced method is more significant owing to the fabrication of many micropatterned samples with a reusable insulated tool. In this research work, SU-8 2150 mask is re-used many times and produced high quality micropatterns. The developed upward perpendicular cross flow system is utilized for identical micropattern production. Micropatterned properties such as material removal rate (MRR), width overcut, depth, and surface roughness (Ra) are influenced by EMM process variables such as voltage, machining time, inter-electrode gap (IEG), and electrolyte concentration. In addition, to determine the optimal parametric mix, an effective methodology known as Measurement of Alternatives and Ranking according to Compromise Solution (MARCOS) is used. The attained optimum process variables are voltage of 10V, IEG of 100 μ m, concentration of 15g/l, and machining time of 3 min for creation of good quality micropatterns. In addition, validation experimentation is conducted at identified optimal parametric values that confirm improved machining performance.

Keywords: Maskless EMM, micropattern, SU-8 2150 mask, MARCOS, MRR, machining accuracy, depth, Ra

1. Introduction

Microtexturing and its distinctive attributes have been played a prominent role in machine-driven equipment [1]. For instance, micropatterned surfaces lower rubbing and abrasion between engineering parts by storing debris particles and enhancing lubrication. Micropatterned surfaces have been extensively used as anti-reflective substances. Micropatterned surfaces are also applied in biomedical, aerospace, automobile applications, etc. [2]. Furthermore, microtextured surfaces enhance evaporation efficiency for spray cooling. Linear micropatterns, for example, are widely used to improve frictional characteristics. Different unconventional micromachining methods have been successfully utilized for producing various types of micropatterns, viz. abrasive jet machining, electrochemical machining, chemical etching, etc. [3]. Maskless electrochemical micromachining (EMM) is a prominent technique with several advantages, viz. higher machining rate, free from tool wear, cracks, heat-affected layer, and residual stress, etc.

Maskless EMM is a promising method with the above-mentioned several advantages compared to other micromachining techniques. A tool electrode having 275 μ m

diameter is applied to fabricate a micro dimple with 300 μ m diameter and 5 μ m depth [4]. Micro dimples are fabricated using jet electrochemical machining, which provides jet current to the confined area for good localization [5]. The productivity of micro dimples fabrication is quite less because the impressions of micropattern is produced individually. Through-mask electrochemical micromachining (TMEMM) process is used to machine 3D microstructures [6]. Though, this method is complicated due to the use of lithographic techniques having several stages for generating textured workpieces before machining. In TMEMM method, an inert film is formed on Ti, which performs as insulation, and laser medium is applied to manufacture patterns. Micro dimples are generated on titanium using the electrochemical machining method [7]. TMEMM is used to make micro dimples on a tubular surface after a dry-film coating is applied [8]. In the modified TMEMM, through holes insulation sheet covered with a conductive layer, used as a non-conductive layer is utilized to produce micro dimples [9]. Additionally, the process has low production efficiency. Polydimethylsiloxane (PDMS) is extensively used in many applications such as lab-on-a-chip research, having several advantages, viz. chemical inertness, inexpensive, and higher flexibility. PDMS masked micro through-holes have been fabricated for microfluidic applications [10]. PDMS masked through-holes are used to create micro-structures using EMM [11]. In

*E-mail address: sandip.sandip.kunar@gmail.com

ISSN: 1791-2377 © 2022 School of Science, IJU. All rights reserved.

doi:10.25103/jestr.155.22

TMEMM, the mask is used on the job for making the insulated pattern and after machining, the mask is removed. In this process, a reusable insulation is developed for machining [12]. In TMEMM, an investigation is directed to explore the effect of duty ratio on performance characteristics of micro-dimples [13]. Maskless EMM method is applied to create the rectangular micropatterns and to investigate the result of process variables on the generated appearances using three pulse waveforms [14]. It is a promising method for fabricating micro dimples and the influences of machining inputs on performance criteria, viz. depth and machining accuracy for different electrolytes [15]. Femtosecond laser with chemical etching process is utilized for fabricating micro dimples on cylindrical and planar surfaces [16, 17]. This method has the thermal effect, which deteriorates the dimensional accuracy of textured patterns.

In maskless EMM, the mask is applied on the micropatterned tool using the lithography process, which provides good adhesion strength between the mask and stainless-steel sheets, obviously restricting the exposure region for flowing the constricted current on the job surface for fabricating the linear micropatterns. Hence, it is significant that this system is used to generate excellent adhesion strength between the SU-8 2150 mask and stainless-steel sheets, thus enhancing the quality of linear micropatterns formed by this maskless EMM method. Because of the chemical inertness and good adhesion strength of the mask, this mask has also excellent potentiality for fabricating good quality linear micropatterns.

This research work explores the fabrication of linear micropattern with a developed electrolyte flow scheme using maskless EMM technique. The developed micropatterning setup has micropatterning cells, developed electrolyte flow scheme, and electrical connection. One masked micropatterned tool can fabricate many high-quality micropatterned samples. Experiments are conducted to reveal the machining influence of voltage, machining time, electrolyte concentration, and IEG on micropatterned features such as MRR, machining depth, width overcut (WO), and surface roughness (R_a) of micropattern. Moreover, an effective approach i.e., MARCOS method is utilized to find the optimal combination of process variables. A confirmation experiment is also carried out based on the obtained optimal parametric mix which reveals that the adopted method can effectively enhance the machining quality thus enhancing the machining performance. Analysis of variance (ANOVA) results further identify the contribution of each of the process parameters accountable for determining the machining quality.

2. Materials and methods

2.1. Experimental details

The developed micropatterning setup is utilized for the production of linear micropattern as shown in Figure 1. It has a microtextured cell, electrical connection, and electrolyte flow scheme for investigation. The cell has fixtures of electrodes, a restricted flow scheme, and an electrical connection facility. This cell arrangement is made at a low cost and produced with corrosion free material i.e., Perspex and stainless steel. The restricted upright cross flow electrolyte system is the most crucial characteristics for fabricating the précised linear micropattern. Because of the restricted flow, there is increased back pressure in the

micropatterning zone, which is better for removing the reactive products from the micromachining zone during the continuous machining process. The current is provided from the pulsed DC electrical unit, which is integrated with an in-built protection function. The micropatterning cell with integrated accessories has been shown in Figure 2. For masking on the micropatterned tool, SU-8 2150 coating is utilized on stainless steel sheets. UV exposure system is employed for making the masked micropattern on stainless steel sheets. The mask thickness of linear micropattern is $208\mu\text{m}$. The width of the linear impression is $445\mu\text{m}$. The inter-electrode gap is controlled by the precision micrometre.

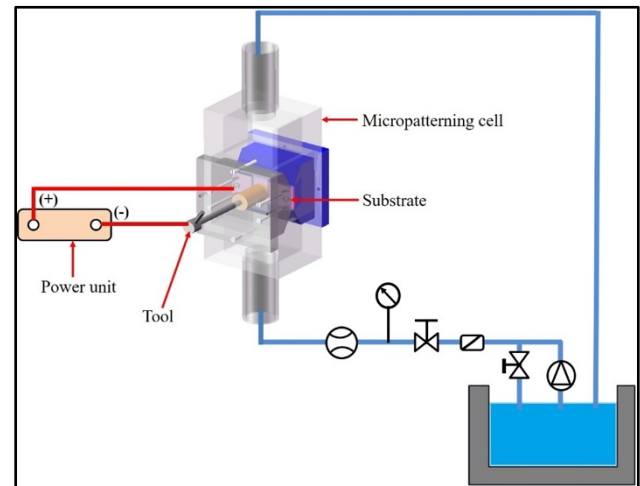


Fig. 1. Micropatterning setup

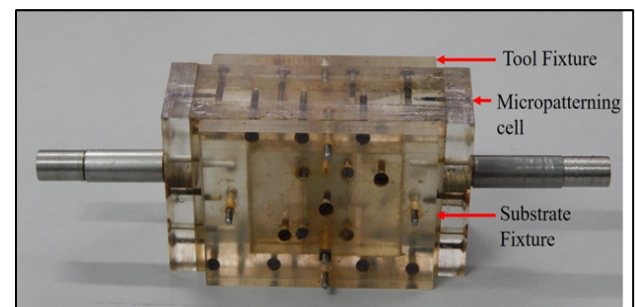


Fig. 2. Micropatterning cell

For proper applicability of this method in advanced fields, the significant process parameters are chosen to explore the machining influence on output features, viz., MRR, surface roughness, width overcut (WO), depth, and (R_a) during micropatterning. The substantial input variables are selected based on widespread trial experiments. Experiments are conducted on stainless steels (SS-304) using a one-time approach at a time. The imperative variables viz. voltage, IEG, electrolyte concentration, and machining time are varied from 8 to 14V, 100 to $250\mu\text{m}$, 15 to 30g/l, and 2 to 5 minutes, respectively as provided in Table 1. Other variables are fixed such as 30% duty ratio, $3.75\text{ m}^3/\text{hr}$ electrolyte flow rate, and 20kHz frequency. The combined electrolyte of NaNO_3 (50%) and NaCl (50%) is used for investigation. In total 13 experiments are conducted at different parametric settings and the response values measured are given in Table 2. The micropatterned characteristics are measured using an optical microscope and 3D Non-Contact Profilometer.

Table 1. EMM process parameters with levels

| Process parameter | Unit | Level 1 | Level 2 | Level 3 | Level 4 |
|-------------------------------|------|---------|---------|---------|---------|
| Voltage (A) | V | 8 | 10 | 12 | 14 |
| Inter electrode gap (B) | µm | 100 | 150 | 200 | 250 |
| Electrolyte Concentration (C) | g/l | 15 | 20 | 25 | 30 |
| Machining time (D) | sec | 2 | 3 | 4 | 5 |

Table 2. Experimental details

| Exp. no. | A | B | C | D | MRR (mg/min) | WO (µm) | Depth (µm) | R _a (µm) |
|----------|----|-----|----|---|--------------|---------|------------|---------------------|
| 1 | 8 | 100 | 15 | 2 | 2.6 | 22.2 | 9.3 | 0.0243 |
| 2 | 10 | 100 | 15 | 2 | 2.8 | 25.6 | 12.1 | 0.0289 |
| 3 | 12 | 100 | 15 | 2 | 3.2 | 42.5 | 13.6 | 0.0321 |
| 4 | 14 | 100 | 15 | 2 | 4.6 | 54.8 | 15.3 | 0.0452 |
| 5 | 8 | 150 | 15 | 2 | 2.4 | 32.8 | 8.5 | 0.0267 |
| 6 | 8 | 200 | 15 | 2 | 2.2 | 39.9 | 8.2 | 0.0342 |
| 7 | 8 | 250 | 15 | 2 | 1.1 | 44.3 | 7.3 | 0.0433 |
| 8 | 8 | 100 | 20 | 2 | 2.8 | 32.1 | 10.6 | 0.0345 |
| 9 | 8 | 100 | 25 | 2 | 3.4 | 45.2 | 11.4 | 0.0453 |
| 10 | 8 | 100 | 30 | 2 | 4.4 | 56.3 | 12.4 | 0.0674 |
| 11 | 8 | 100 | 15 | 3 | 2.9 | 27.4 | 12.4 | 0.0342 |
| 12 | 8 | 100 | 15 | 4 | 3.8 | 34.4 | 13.4 | 0.0356 |
| 13 | 8 | 100 | 15 | 5 | 4.1 | 52.1 | 17.8 | 0.0765 |

2.2. Measurement of alternatives and ranking according to Compromise Solution (MARCOS) method

The MARCOS method is a recent, simple, and effective multi-criteria decision-making method used for ranking various alternatives and optimization of the process [18]. The mathematical foundation of MARCOS depends on describing the interrelationship between the criteria values of alternatives with respect to their ideal and anti-ideal values. Based on those defined relationships, the utility functions of the considered alternatives are computed and subsequently ranked using a compromised ranking method in relation to ideal and anti-ideal solutions. The utility function defines the closeness of an alternative with respect to the ideal and anti-ideal solutions. The alternative which is closest to the ideal and furthest from the anti-ideal is considered to be the best choice. The application of MARCOS method is explained in the following steps:

Step 1: Construction of initial decision matrix

$$X = \begin{matrix} & C_1 & C_2 & \dots & C_n \\ A_1 & x_{11} & x_{12} & \dots & x_{1n} \\ A_2 & x_{21} & x_{22} & \dots & x_{2n} \\ \dots & \dots & \dots & \dots & \dots \\ A_m & x_{m1} & x_{m2} & \dots & x_{mn} \end{matrix} \quad (1)$$

where x_{ij} is the performance measure of i^{th} alternative (A_i) against j^{th} criterion (C_j), m is the number of alternatives and n is the number of criteria/attributes.

Step 2: Development of extended initial matrix

The extended initial matrix can be developed by identifying the ideal (AI) and the anti-ideal (AAI) values for each criterion in the decision matrix as follows:

$$X = \begin{matrix} & C_1 & C_2 & \dots & C_n \\ AAI & x_{aa1} & x_{aa2} & \dots & x_{aan} \\ A_1 & x_{11} & x_{12} & \dots & x_{1n} \\ A_2 & x_{21} & x_{22} & \dots & x_{2n} \\ \dots & \dots & \dots & \dots & \dots \\ A_m & x_{m1} & x_{m2} & \dots & x_{mn} \\ AI & x_{ai1} & x_{ai2} & \dots & x_{ain} \end{matrix} \quad (2)$$

The AAI is the worst alternative consisting of all the non-ideal criteria values whereas on the other hand, AI is the alternative with the best characteristics as it consists of the ideal criteria values. Based on the type of criteria characteristics the AAI and AI can be obtained for each criterion as

For beneficial criteria

$$AAI = \min_i x_{ij} \text{ and } AI = \max_i x_{ij} \quad (3)$$

For non-beneficial criteria

$$AAI = \max_i x_{ij} \text{ and } AI = \min_i x_{ij} \quad (4)$$

Step 3: Normalization of the extended initial matrix

The element of extended initial matrix is normalized using the following formulae:

$$N = [n_{ij}]_{m \times n} \quad (5)$$

$$n_{ij} = \frac{x_{ij}}{x_{ai}} \quad (\text{for beneficial criteria})$$

$$n_{ij} = \frac{x_{ai}}{x_{ij}} \quad (\text{for non-beneficial criteria})$$

Step 4: Development of weighted normalized matrix

The weighted normalized matrix can be obtained as

$$Z = [z_{ij}]_{m \times n} \quad (6)$$

$$z_{ij} = n_{ij} \times w_j$$

where w_j is the weights calculated for each criterion.

Step 5: Computation of utility degree (K_i) for each alternative

The utility degree for each alternative can be calculated with reference to the ideal and anti-ideal solution as

$$K_i^+ = \frac{S_i}{S_{ai}} \quad (7)$$

$$K_i^- = \frac{S_i}{S_{aai}} \quad (8)$$

where S_i is sum of weighted normalized matrix obtained as

$$S_i = \sum_{j=1}^n v_{ij}$$

Step 6: Calculation of utility function $f(K_i)$ for each alternative

The utility function for each alternative can be calculated as a compromise of the observed alternatives with reference to the ideal and anti-ideal solution as given below:

$$f(K_i) = \frac{K_i^+ + K_i^-}{1 + \frac{1 - f(K_i^+)}{K_i^+} + \frac{1 - f(K_i^-)}{K_i^-}} \quad (9)$$

Where $f(K_i^+)$ and $f(K_i^-)$ are the utility function calculated based on the ideal and anti-ideal solution. These can be calculated as

$$f(K_i^+) = \frac{K_i^+}{K_i^+ + K_i^-}$$

$$f(K_i^-) = \frac{K_i^-}{K_i^+ + K_i^-}$$

The alternative with the highest value of utility function is identified as the best choice among all considered alternatives.

3. Results and discussion

3.1. Influence of process variables on micropatterned characteristics

An investigation is performed to explore the effect of machining voltage on performance criteria i.e., MRR, depth, width overcut, and R_a with other constant parameters i.e., 100 μ m IEG, 15g/l electrolyte concentration, and 2 min

machining time and variations are shown in Figure 3. Because of the increasing machining current, the MRR rises as the voltage rises. Higher current leads to a higher machining rate throughout the patterned area. As the voltage rises, the stray current effect increases, causing machining precision to diminish. The micropatterned depth increases due to better machining localization with higher voltage. Because of the non-uniform etching for higher voltage, there is more surface roughness. Hence, for generating précised linear micropattern, lower voltage is suggested.

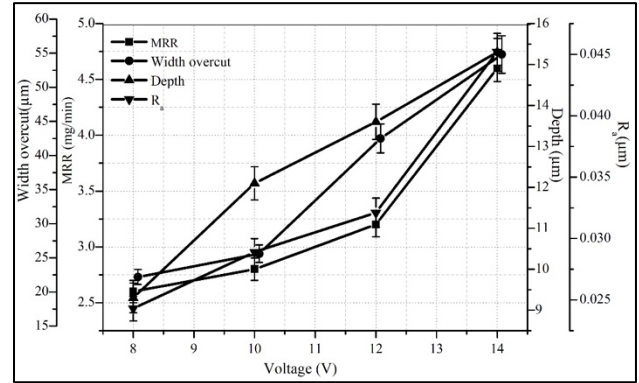


Fig. 3. Variation of MRR, WO, depth and R_a with voltage

The machining influence of electrolyte concentration is investigated on micropatterned features with other fixed parameters, viz. 8V voltage, 100 μ m IEG, and 2 min machining time and the responses are shown in Figure 4. Because of the greater machining current, the MRR rises as the electrolyte concentration rises, assisting in the removal of more material from the micropatterning zone. The width overcut rises owing to the distribution of uncontrolled current flux with higher concentration. The micropatterned depth rises because of the controlled distribution of current density with higher electrolyte concentration. The surface finish lowers due to irregular etching with electrolyte concentration. Therefore, for obtaining a good linear micropattern, a lower electrolyte concentration is suggested.

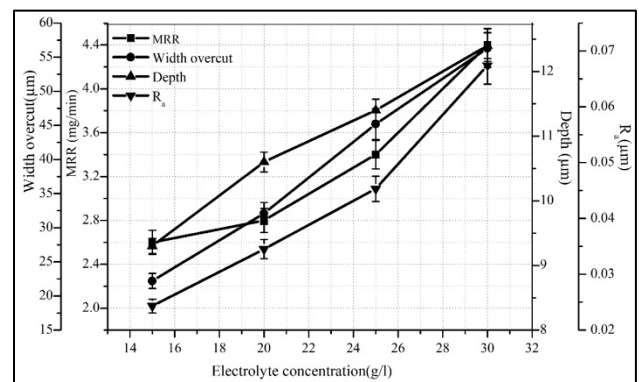


Fig. 4. Variation of MRR, WO, depth and R_a with electrolyte concentration

Experiments with other fixed parameters, such as 15 g/l electrolyte concentration, 8V voltage, and 2 min machining time, are carried out to reveal the effect of IEG on surface properties, and responses are plotted in Figure 5. Because of greater ohmic resistance and unregulated current flux distribution, the MRR decreases as IEG increases. The width overcut rises with greater IEG because of uncontrolled stray current effect. The depth reduces with higher IEG due to lower machining localization. Due to uneven milling,

surface roughness increases as IEG increases. Hence, for accurate linear micropattern, lower IEG is suggested.

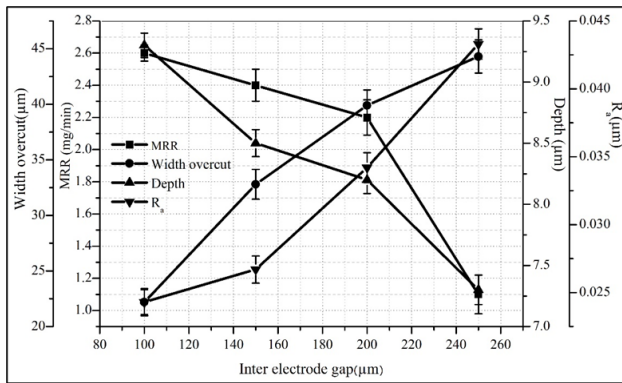


Fig. 5. Variation of MRR, WO, depth and R_a with IEG

Figure 6 depicts the effect of machining time on performance criteria when other fixed parameters such as electrolyte concentration of 15 g/l, a voltage of 8 V, and IEG of 100 m are used. Because of the regulated machining, the MRR increases as the machining time increases. The width overcut increases as the machining time increases due to increased stray current influence. Surface roughness increases with increased machining time due to uncontrolled anodic dissolution. As a result, a shorter machining time is suggested for creating a regular linear micropattern.

3.2. Parametric optimization using MARCOS method

The present section illustrates the application of MARCOS method in finding the best parametric setting for the EMM process. The experimental details presented in Table 2 are employed to apply this novel approach to determine the optimal process parametric combination of voltage, IEG, electrolyte concentration, and machining time to obtain maximum MRR and machining depth as well as minimum WO and R_a during fabrication of linear micro patterns on SS304 workpiece.

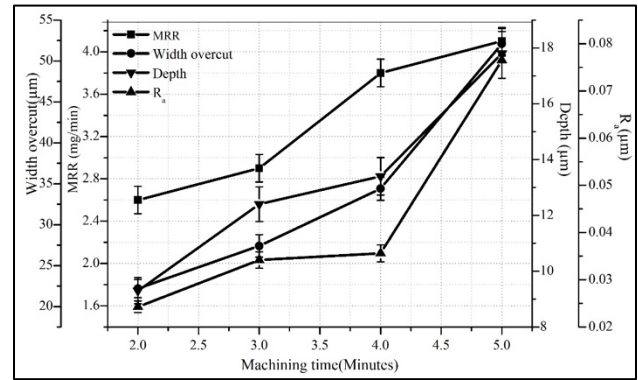


Fig. 6. Variation of MRR, WO, depth and R_a with machining time

Among the three considered responses, MRR and depth are of beneficial type quality characteristics, and overcut and R_a are of non-beneficial type quality characteristics. Based on the experimental results provided in Table 2, the extended initial matrix of machining responses is developed by using Equations (2), (3), and (4) by identifying the ideal (AI) and anti-ideal (AAI) values as described in step 2. The ideal values for MRR, WO, machining depth, and surface roughness were identified to be 4.6, 22.2, 17.8, and 0.0243, respectively. On the other hand, the anti-ideal values for MRR, WO, machining depth, and surface roughness are obtained as 1.1, 56.3, 7.3, and 0.0765, respectively. In the next step, employing Equation (5), normalization of the extended initial matrix is carried out. These normalized values of the initial matrix are subsequently multiplied with the weights calculated for each criterion to obtain a weighted normalized matrix as per Equation (6) shown in step (4). The entropy method is used to calculate the weight of each output characteristic of the electrochemical micromachining process, such as MRR, WO, machining depth, and surface roughness. The entropy weights of MRR, WO, machining depth, and surface roughness are estimated as 0.1837, 0.3262, 0.3194, and 0.1707, respectively. The normalized and weighted normalized matrix for each response is presented in Table 3.

Table 3. Normalized and weighted normalized matrix for each response

| | Normalized matrix | | | | Weighted normalized matrix | | | |
|-----|-------------------|--------|--------|--------|----------------------------|--------|--------|--------|
| | MRR | WO | Depth | R_a | MRR | WO | Depth | R_a |
| AAI | 0.2391 | 0.3943 | 0.4101 | 0.3176 | 0.0439 | 0.1286 | 0.131 | 0.0542 |
| 1 | 0.5652 | 1 | 0.5225 | 1 | 0.1038 | 0.3262 | 0.1669 | 0.1707 |
| 2 | 0.6087 | 0.8672 | 0.6798 | 0.8408 | 0.1118 | 0.2829 | 0.2171 | 0.1435 |
| 3 | 0.6957 | 0.5224 | 0.764 | 0.757 | 0.1278 | 0.1704 | 0.244 | 0.1292 |
| 4 | 1 | 0.4051 | 0.8596 | 0.5376 | 0.1837 | 0.1321 | 0.2745 | 0.0918 |
| 5 | 0.5217 | 0.6768 | 0.4775 | 0.9101 | 0.0958 | 0.2208 | 0.1525 | 0.1554 |
| 6 | 0.4783 | 0.5564 | 0.4607 | 0.7105 | 0.0879 | 0.1815 | 0.1471 | 0.1213 |
| 7 | 0.2391 | 0.5011 | 0.4101 | 0.5612 | 0.0439 | 0.1635 | 0.131 | 0.0958 |
| 8 | 0.6087 | 0.6916 | 0.5955 | 0.7043 | 0.1118 | 0.2256 | 0.1902 | 0.1202 |
| 9 | 0.7391 | 0.4912 | 0.6404 | 0.5364 | 0.1358 | 0.1602 | 0.2046 | 0.0916 |
| 10 | 0.9565 | 0.3943 | 0.6966 | 0.3605 | 0.1757 | 0.1286 | 0.2225 | 0.0615 |
| 11 | 0.6304 | 0.8102 | 0.6966 | 0.7105 | 0.1158 | 0.2643 | 0.2225 | 0.1213 |
| 12 | 0.8261 | 0.6453 | 0.7528 | 0.6826 | 0.1518 | 0.2105 | 0.2404 | 0.1165 |
| 13 | 0.8913 | 0.4261 | 1 | 0.3176 | 0.1637 | 0.139 | 0.3194 | 0.0542 |
| AI | 1 | 1 | 1 | 1 | 0.1837 | 0.3262 | 0.3194 | 0.1707 |

Equations (7) and (8) are employed to estimate the utility degree of alternatives. Finally, the utility function for each experimental run is estimated using Equation (9). Based on obtained utility function score $[f(K_i)]$, ranking of each experimental run is carried out to identify the best suitable process parametric combination among all thirteen

experimental runs considered in the present research investigation. Table 4 presents the sum of the elements of the weighted matrix, utility degree, and utility function for each experimental run. The highest $f(K_i)$ value is obtained in experiment No. 1 of the electrochemical micromachining process parametric combination, as shown in the same table.

As a result, among the thirteen experiments, experiment no. 1 has the best process parametric settings during the fabrication of linear micro patterns on SS304 work material

for the best multi-performance characteristics or desirable output responses.

Table 4. Sum of the elements of the weighted matrix, utility degree and utility function for each experimental trial

| | Si | Ki- | Ki+ | f(Ki-) | f(Ki+) | f(Ki) | Rank |
|------------|---------------|--------|--------|--------|--------|--------|------|
| AAI | 0.3578 | | | | | | |
| 1 | 0.7676 | 2.1456 | 0.7676 | 0.2635 | 0.7365 | 0.7015 | 1 |
| 2 | 0.7553 | 2.1113 | 0.7553 | 0.2635 | 0.7365 | 0.6903 | 2 |
| 3 | 0.6714 | 1.8768 | 0.6714 | 0.2635 | 0.7365 | 0.6136 | 7 |
| 4 | 0.6822 | 1.9067 | 0.6822 | 0.2635 | 0.7365 | 0.6234 | 6 |
| 5 | 0.6245 | 1.7456 | 0.6245 | 0.2635 | 0.7365 | 0.5707 | 9 |
| 6 | 0.5378 | 1.5032 | 0.5378 | 0.2635 | 0.7365 | 0.4914 | 12 |
| 7 | 0.4342 | 1.2136 | 0.4342 | 0.2635 | 0.7365 | 0.3968 | 13 |
| 8 | 0.6479 | 1.8108 | 0.6479 | 0.2635 | 0.7365 | 0.592 | 8 |
| 9 | 0.5921 | 1.655 | 0.5921 | 0.2635 | 0.7365 | 0.5411 | 11 |
| 10 | 0.5884 | 1.6446 | 0.5884 | 0.2635 | 0.7365 | 0.5377 | 10 |
| 11 | 0.7239 | 2.0234 | 0.7239 | 0.2635 | 0.7365 | 0.6615 | 3 |
| 12 | 0.7192 | 2.0103 | 0.7192 | 0.2635 | 0.7365 | 0.6573 | 4 |
| 13 | 0.6763 | 1.8905 | 0.6763 | 0.2635 | 0.7365 | 0.6181 | 5 |
| AI | 1 | | | | | | |

However, to find an optimal process parameter setting, the average $f(K_i)$ values for the respective level of input parameters based on the experimental plan were determined by considering the average of various $f(K_i)$ values at the same variable level for the respective column. Table 5 and Figure 7 show the average $f(K_i)$ values for the various important EMM parameters considered in the current experimental investigation. A higher $f(K_i)$ value indicates better machining performance regardless of the type of micro-pattern characteristics. As a result, the optimal setting for a micro-texturing process parametric combination is the one with the highest $f(K_i)$ value. The optimum setting for EMM process during fabrication of micro-pattern of SS304 was determined using the $f(K_i)$ values described in Table 5: 10V voltage (level 2), 100 μm IEG (level 1), 15 g/l electrolyte concentration (level 1), and machining time 3

min (level 2). The differences among the greater and the smaller values of the utility degree of EMM process parameters are 0.1135 for voltage, 0.2268 for IEG, 0.0648 for electrolyte concentration, and 0.0856 for machining time. Furthermore, the differences between larger and smaller $f(K_i)$ values for different parameters are compared at all four levels to determine the most important factor affecting output characteristics. This evaluation determines the order of significance of the parameters to the multi-performance characteristics. The highest value indicates the most influencing process parameters. From the table, the highest value of 0.2268 corresponding to IEG, establishes the fact that the IEG has the uppermost impact on the multi-performance characteristics amongst all the EMM process parameters.

Table 5. Response table for utility function

| Process parameter | Unit | Level 1 | Level 2 | Level 3 | Level 4 |
|-------------------------------|---------------|---------------|---------------|---------|---------|
| Voltage (A) | V | 0.5768 | 0.6903 | 0.6136 | 0.6234 |
| IEG (B) | μm | 0.6236 | 0.5707 | 0.4914 | 0.3968 |
| Electrolyte Concentration (C) | g/l | 0.6025 | 0.5920 | 0.5411 | 0.5377 |
| Machining time (D) | sec | 0.5759 | 0.6615 | 0.6573 | 0.6181 |

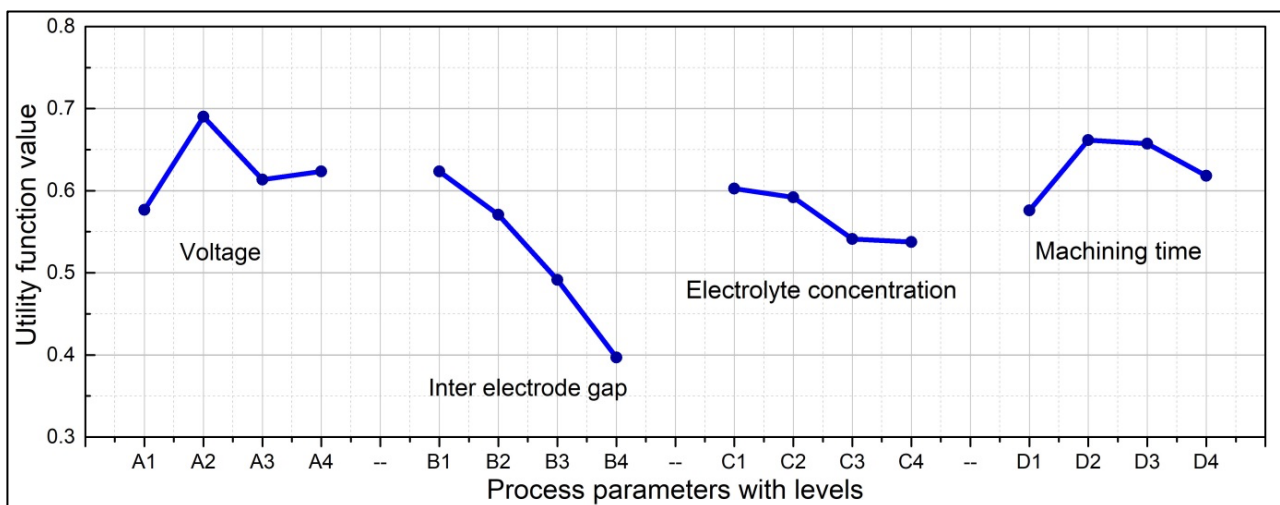


Fig. 7. Response graph for utility function

3.3. Confirmation experiment

A validation experiment is performed to validate the optimal process parametric combination i.e., voltage as 10V, IEG as 100 μm , electrolyte concentration as 15 g/l, and machining time as 3 min during the production of micropatterns on SS304. The measured performance characteristics obtained employing the obtained optimal parametric mix is shown in Table 6. For generating the linear micropattern, the SU-8 2150 masked tool is utilized to produce many high quality micropatterns without distortion of the mask because of higher strength of the masked tool, higher resistance capability of the mask, etc. The micropattern is identical throughout the micromachining area due to controlled anodic dissolution. Because of the reduced stray current effect, machining precision is also improved. Due to homogeneous disintegration, the micropatterned depth is nearly consistent throughout the pattern. Because of the regulated etching in the pattern, the surface finish also improves. From the validation experiment, it is evident that the optimal process parametric combination obtained using MARCOS method produces better response values compared to other experimental results thus improving the machining quality.

Table 6. Comparison between initial and optimal response values

| Response | Initial setting (A1B1C1D1) | MARCOS method (A2B1C1D2) |
|---------------------------|----------------------------|--------------------------|
| MRR (mg/min) | 2.6 | 2.93 |
| Overcut (μm) | 22.2 | 23.5 |

| | | |
|-------------------------|--------|--------|
| Depth (μm) | 9.3 | 13.1 |
| R_a (μm) | 0.0243 | 0.0237 |

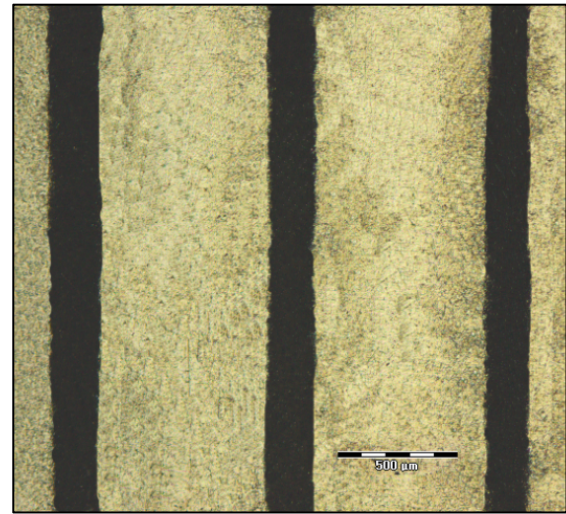


Fig. 8. Regular linear micropattern

The microscopic image of linear micropattern is generated at the optimal parametric combination as shown in Figure 8. The 3D image of the micro linear impression with depth profile is shown in Figure 8 having a depth of 19.4 μm and the 2D roughness profile with a value of 1.07 nm is illustrated through Figure 9.

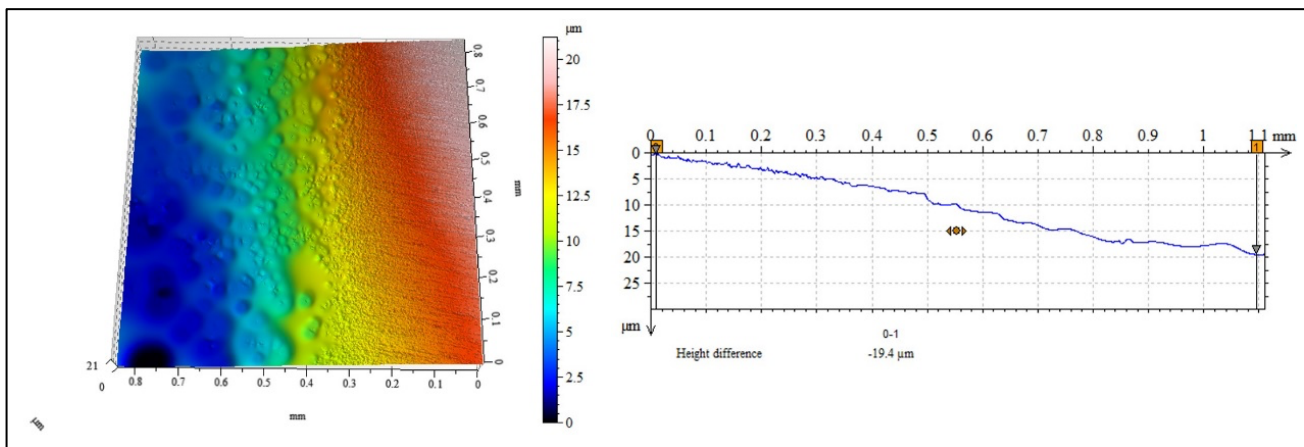


Fig. 9. 3D profile with 2D depth profile

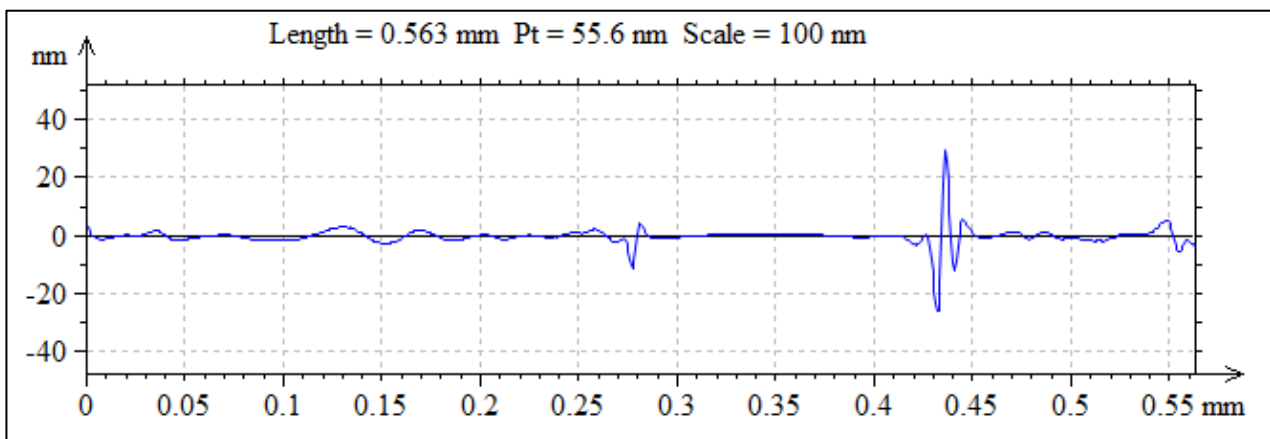


Fig. 10. Roughness profile

3.4. ANOVA results

To identify the significance of each EMM process parameter on the calculated utility function scores, ANOVA is implemented, and the results are shown in Table 7. It is noticed from the table that the degree of freedom (DOF) for the residual error is obtained a value of zero signifying insufficient data to carry out the analysis. Typically, it occurs when there four process parameters and the number of experiments is comparatively less. To overcome such error, pooling is performed [19]. Pooling is a process of revising and re-estimating the ANOVA results to omit a factor having less significance as compared to other factors. It can be observed from Table 7, that machining time having a minimum adjusted mean square (Adj. MS) value of 0.001162 as compared to others can be recognized as the least influencing factor. Hence, machining time is pooled from Table 8. In ANOVA analysis, *p*-value less than or equal to 0.05 is statistically significant, or else it is not. The results provided in Table 8 indicate that IEG is the most influential factor followed by electrolytic concentration and voltage supporting the above findings.

Table 7. ANOVA results for utility function scores (before pooling)

| Source | DOF | Adj SS | Adj MS | <i>f</i> -value | <i>p</i> -value |
|---------------------------|-----|----------|----------|-----------------|-----------------|
| Voltage | 3 | 0.006102 | 0.002034 | * | * |
| Inter electrode gap | 3 | 0.049893 | 0.016631 | * | * |
| Electrolyte Concentration | 3 | 0.017525 | 0.005842 | * | * |
| Machining time | 3 | 0.003487 | 0.001162 | * | * |
| Error | 0 | * | * | | |
| Total | 12 | 0.087098 | | | |

Table 8. ANOVA results for utility function scores (after pooling)

| Source | DOF | Adj SS | Adj MS | <i>f</i> -value | <i>p</i> -value |
|---------------------------|-----|----------|----------|-----------------|-----------------|
| Voltage | 3 | 0.003990 | 0.001330 | 1.14 | 0.457 |
| Inter electrode gap | 3 | 0.066645 | 0.022215 | 19.11 | 0.019 |
| Electrolyte Concentration | 3 | 0.019920 | 0.006640 | 5.71 | 0.093 |
| Error | 3 | 0.003487 | 0.001162 | | |
| Total | 12 | 0.087098 | | | |

4. Conclusions

For producing high-quality linear micropatterns, an unconventional method, called maskless EMM is used. The machining influence of EMM process variables on micropatterned characteristics is explored and the MARCOS method is employed to accomplish the optimal parametric combination for achieving high-quality linear micropattern. From the above-mentioned analysis, the following conclusions can be drawn:

- (i) An effective method is used to conduct the experimentation using a developed investigational setup. One insulated patterned tool can produce many high-quality patterned samples without distortion of the mask.
- (ii) Machining with lower IEG, lower electrolyte concentration, lower voltage, and shorter machining time is advised for higher machining rate and dimensional accuracy.
- (iii) MARCOS method is used to ascertain the optimum process parameters to achieve higher MRR and machining depth and lower WO and R_a from various parametric combinations used in the present experimental investigation.
- (iv) The optimal parametric combination for maskless EMM during micropatterning on SS304 is obtained as 100 μm IEG, 10 V voltage, 15 g/l electrolyte concentration, and 3 min machining time. In addition, the justification experiment using the attained optimal process variables is corroborated with the novel approach and framework used in the present investigation to boost the overall micropatterning operation.

Furthermore, extensive study may be carried out in the development of intricate masked tool design and micro texturing on curved surfaces for advanced microengineering application.

This is an Open Access article distributed under the terms of the Creative Commons Attribution License.



References

1. Bruzzone, A.A.G., Costa, H.L., Lonardo, P.M. and Lucca, D.A., 2008. Advances in engineered surfaces for functional performance. *CIRP annals*, 57(2), pp.750-769.
2. Qu, N.S., Qian, W.H., Cai, W.Z., Xing, Z.H., Zhu, Z.W. and Zeng, Y.B., 2013. Fabrication of microprism mould by electroforming with high electrolyte flowrate. *Transactions of the IMF*, 91(4), pp.221-224.
3. Kunar, S., Mahata, S. and Bhattacharyya, B., 2018. Influence of electrochemical micromachining process parameters during fabrication of varactor micropattern. *The International Journal of Advanced Manufacturing Technology*, 96(1), pp.411-427.
4. Byun, J.W., Shin, H.S., Kwon, M.H., Kim, B.H. and Chu, C.N., 2010. Surface texturing by micro-ECM for friction reduction. *International Journal of Precision Engineering and Manufacturing*, 11(5), pp.747-753.
5. Hackert-Oschätzchen, M., Martin, A., Meichsner, G., Zinecker, M. and Schubert, A., 2013. Microstructuring of carbide metals applying Jet Electrochemical Machining. *Precision Engineering*, 37(3), pp.621-634.
6. Li, W., Quandt, W., Xiuqing, H., Yucheng, D. and Bingheng, L., 2010. Finite element simulation and experimental study on the through-mask electrochemical micromachining (EMM) process. *The International Journal of Advanced Manufacturing Technology*, 51(1-4), pp.155-162.
7. Chauvy, P.F., Hoffmann, P. and Landolt, D., 2001. Electrochemical micromachining of titanium through a laser patterned oxide film. *Electrochemical and Solid State Letters*, 4(5), p.C31.
8. Qu, N., Chen, X., Li, H. and Zeng, Y., 2014. Electrochemical micromachining of micro-dimple arrays on cylindrical inner surfaces using a dry-film photoresist. *Chinese Journal of Aeronautics*, 27(4), pp.1030-1036.
9. Qian, S., Zhu, D., Qu, N., Li, H. and Yan, D., 2010. Generating micro-dimples array on the hard chrome-coated surface by modified through mask electrochemical micromachining. *The International Journal of Advanced Manufacturing Technology*, 47(9-12), pp.1121-1127.
10. Santisteban, T.S., Zengerle, R. and Meier, M., 2014. Through-holes, cavities and perforations in polydimethylsiloxane (PDMS) chips. *RSC advances*, 4(89), pp.48012-48016.
11. Chen, X., Qu, N., Li, H. and Zhu, D., 2014. The fabrication and application of a PDMS micro through-holes mask in electrochemical micromanufacturing. *Advances in Mechanical Engineering*, 6, p.943092.

12. Zhu, D.N.S.Q., Qu, N.S., Li, H.S., Zeng, Y.B., Li, D.L. and Qian, S.Q., 2009. Electrochemical micromachining of microstructures of micro hole and dimple array. *CIRP annals*, 58(1), pp.177-180.
13. Mahata, S., Kunar, S. and Bhattacharyya, B., 2018. Micro dimple array fabrication by through mask electrochemical micromachining utilizing low-aspect ratio mask. *Journal of The Electrochemical Society*, 165(3), p.E129.
14. Kunar, S. and Bhattacharyya, B., 2021. Influence of various pulse waveforms during fabrication of micro rectangular pattern by masked tool using electrochemical micromachining. *Journal of Advanced Manufacturing Systems*, 20(01), pp.27-50.
15. Kunar, S., Rajkeerthi, E., Mandal, K. and Bhattacharyya, B., 2020. Fabrication of array of micro circular impressions using different electrolytes by maskless electrochemical micromachining. *Manufacturing Review*, 7, p.15.
16. Chen, F., Liu, H., Yang, Q., Wang, X., Hou, C., Bian, H., Liang, W., Si, J. and Hou, X., 2010. Maskless fabrication of concave microlens arrays on silica glasses by a femtosecond-laser-enhanced local wet etching method. *Optics express*, 18(19), pp.20334-20343.
17. Du, G., Yang, Q., Chen, F., Liu, H., Deng, Z., Bian, H., He, S., Si, J., Meng, X. and Hou, X., 2012. Direct fabrication of seamless roller molds with gapless and shaped-controlled concave microlens arrays. *Optics letters*, 37(21), pp.4404-4406.
18. Stević, Ž., Pamučar, D., Puška, A. and Chatterjee, P., 2020. Sustainable supplier selection in healthcare industries using a new MCDM method: Measurement of alternatives and ranking according to COmpromise solution (MARCOS). *Computers & Industrial Engineering*, 140, p.106231.
19. Das, P.P. and Chakraborty, S., 2019. Parametric optimization of non-traditional machining processes using Taguchi method and super ranking concept. *Yugoslav Journal of Operations Research*, 29(2), pp. 249-271.